Offsets in Wavelength Between the Large and Small Science Apertures of the GHRS

A. Schultz, D. Soderblom, S. Hulbert, and L. Sherbert
March 7, 1997

ABSTRACT

The wavelength shifts (offsets) between the GHRS LSA and SSA have been determined from the measured pixel shift for stars observed in both apertures. HD 155763 (ζ Dra) was observed with the first order gratings, while HD 141556 (χ Lupi) was observed with Ech-A and Ech-B, both as GHRS calibration proposal 6213. The target stars were first centered and observed in the LSA followed by slewing the telescope to position the target in the SSA. To eliminate movement of the carrousel between observations, No SSA ACQ/PEAKUPs were performed to center the targets in the SSA. This report summaries the observations, data reductions, and wavelength offset calculations. We find values for these offsets that are significantly different from the values determined in SV, and with better internal precision. Table 9 at the end summarizes these new values.

1. Introduction

Wavelengths are one of the fundamental calibrations provided in routine reduction of spectroscopic observations. With the GHRS, an object may be observed with either the Large Science Aperture (LSA) or Small Science Aperture (SSA). The LSA is used to obtain measurements of stellar fluxes, while the SSA is used to obtain the most precise wavelengths. The SSA is small enough that minor movements of a star in the aperture are unimportant. Due to the higher resolution when using the SSA, the convention for the GHRS is to place wavelengths on a scale appropriate to a star observed in the SSA.

In some circumstances it is important to improve the wavelength scale for an object observed in the LSA. There is a net wavelength shift between the LSA and SSA because light entering them goes through the GHRS optics at slightly different angles. A wavelength calibration exposure may also be obtained. Because of problems with the low-voltage power supply, only the lamp designated SC2 has been used for wavecals since 1991, although lamp SC1 was used for Side 1 observations before that. The relative loca-

tions of the lamp apertures and the science apertures is shown in Figure 1 (see below). The GHRS reduction software **calhrs** is designed to place wavecal exposures on a scale appropriate to the SSA, as noted.

The purpose of the Cycle 5 calibration program 6213 was to measure the wavelength offsets between the LSA and SSA directly. The scheme was to observe a bright star with narrow lines in both apertures, and to then measure the apparent shift in the spectra. To reduce systematic effects, the observing strategy was to first center the star in the LSA, obtain a spectrum, move the star to the SSA, and then observe again at the same wavelength. The star was moved back to the LSA and recentered before the next wavelength was observed. As a result, no carrousel motion occurred during an entire sequence at any one wavelength. To avoid a SPYBAL (which would have moved the carrousel), no peakup was done in the SSA.

The GHRS point spread function (PSF) is comparable to the size of the SSA. A small offset within the SSA results in about half the dispersion offset as a similar positional offset in the LSA. The ratio of the detected counts in the SSA versus the LSA on-average for pairs of observations was nominal, ~50% at 1250 Å to ~70% at 3000 Å. This indicates the wavelength offset due to positioning errors is small, but not negligible.

When the GHRS carrousel is rotated to place a desired wavelength at the center of the diode array, the spectra will be displaced slightly on the photocathode in both the *y*- (LINE) and *x*- (SAMPLE) directions. The exact location of a spectrum on the photocathode will depend upon the carrousel position, and will have some modest thermal and geomagnetic dependencies as well. A change in grating, or a positional shift from the LSA to the SSA, is considered a new alignment and will generate a SPYBAL. A SPYBAL (Spectrum-Y-Balance) observation is commanded at the start of the first science observation. The SPYBAL procedure uses an observation of the spectral calibration lamp and performs a null-deflection in the *y* direction to ensure that the spectrum does not fall off the top or bottom of the diode array. A SPYBAL actually produces science data consisting of a wavelength calibration exposure. The wavelength used is different for each grating and was chosen to give an even distribution of light over the bandpass sampled. The null-deflection determines an offset from the nominal position (telemetry point (ZSPYBLU)) that is subsequently applied to all following science observations until a another SPYBAL is obtained, either after 90 minutes of elapsed alignment time has occurred, a change in grating, or a new alignment. See GHRS ISR 072, ***A Review of the Utility of SPYBALs***, for a more detailed description.

See the ***Instrument Handbook for the Goddard High Resolution Spectrograph*** for a more detailed description of the operation of the GHRS.

2. Wavelength Calibration

GHRS wavelength observations (wavecals) are routinely obtained during each observing cycle to monitor the performance and stability of the GHRS. The results of these monitoring programs are used to check the optical alignment, carrousel position, image deflection, and dispersion coefficients. A standard dispersion equation is used by **calhrs** for data reductions.

The locations of the GHRS apertures relative to the spacecraft axes are displayed in Figure 1. The light from the calibration lamps enters the instrument through different apertures than light from an external target. The GHRS science calibration is referenced to the SSA. **calhrs** computes wavelengths assuming targets are centered in the SSA and applies an offset to the dispersion relationships if the target is in the LSA. An offset is also applied to wavecals.

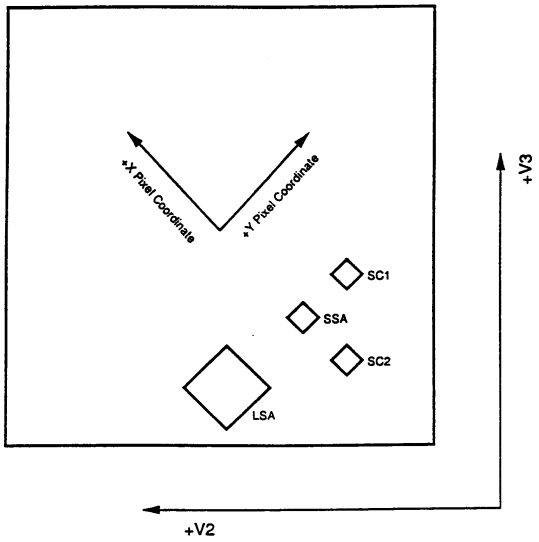

Figure 1: Locations of GHRS Apertures Relative to Spacecraft Axes

The wavelength offsets between the SSA and the calibration lamp apertures were determined during ground based calibrations, while the offsets between the SSA and LSA were determined from on-orbit science observations during SV (science verification). The differences between the SSA and LSA offsets were determined to be less than 0.50 sample units. See the ***Final Report of the Science Verification Program for the GHRS for the Hubble Space Telescope***, Ball Aerospace Systems Group, for details of the GHRS SV program. The limited data obtained during SV did not allow the construction of accurate models of the variations of the offset with carrousel position and sample position.

Table 1 summarizes the useful wavelength range, dispersion, and bandpass for each of the first order gratings. For the echelles, this information can be found in the ***GHRS Instrument Handbook 6.0***, pages 102-103.

Table 1. Useful Wavelength Ranges for First-Order Gratings

Grating	Useful Range (Å)	Dispersion (Å/diode)	Bandpass (Å)	Comment
G140L	1100 – 1900	0.572 – 0.573	286 – 287	
G140M	1100 – 1900	0.056 – 0.052	28 – 26	
G160M	1150 – 2300	0.072 – 0.066	36 – 33	2nd order overlap above 2300 Å
G200M	1600 – 2300	0.081 – 0.075	41 – 38	2nd order overlap above 2300 Å
G270M	2000 – 3300	0.096 – 0.087	48 – 44	2nd order overlap above 3300 Å

The full-width-at-half-maximum (FWHM) measurements of lines from the calibration lamps were used to determine the resolving power of each grating. Tests have shown that the measured FWHM does not change significantly with wavelength for the first-order gratings (Ebbets & Lindler, GHRS-SV-068, 1991).

During calibration, the zero-points of the wavelength scale are adjusted for the difference in incidence angle of apertures LSA, SC1, and SC2 from the SSA. Incident Angle Correction (IAC_CORR) coefficients are found in the ccr8 table. Currently, an average value for the zero-point wavelength correction is applied to all first order grating LSA observations regardless of the carrousel position. The current (old) offsets for the first order gratings are listed in Table 2. These coefficients are used to compute the offset using the following formula: $\lambda = \lambda + (A + Bs)/m$

where:

λ is the wavelength,
A and B are coefficients from `ccr8`,
s is the photocathode sample position, and
m is the spectral order.

Table 2. Current LSA Incident Angle Correction for First-Order Gratings

Grating	Aperture	CARPOS	A	B
G140L	LSA	all	0.0	0.0
G140M	LSA	all	0.0	0.0
G160M	LSA	all	–0.022	0.0
G200M	LSA	all	–0.037	0.0
G270M	LSA	all	–0.036	0.0

No incident angle correction is now applied to LSA Ech-A or Ech-B observations.

3. New Observations

GHRS Cycle 5 calibration program 6213 obtained spectra of the stars ζ Dra (HD 155763) with the first order gratings G140M, G160M, G200M, and G270M, and χ Lupi (HD 141556) with Ech-A and Ech-B. ζ Dra (B6III) was observed as a CVZ target, while

echelle observations of the metal rich star χ Lupi (B9IV) were obtained less efficiently due to Earth occultations. The observations were obtained using ACCUM mode. The wavelength regions covered were chosen to detect narrow absorption lines with some overlap between each grating. The limiting factor in determining the pixel shift between the LSA and SSA will ultimately be the positioning of the targets within the LSA. The location of the SSA from the LSA is well known, and any SSA offset from the first dwell position will be an estimate of the error in LSA centering. Each step in the SSA spiral search is 0.05" (~1/4 diode or 1 pixel). Statistically during Cycles 4, 5, and 6 (post-COSTAR), a target was found one dwell position from the first dwell position in the SSA ACQ/PEAKUP spiral search. This offset corresponds to ~1/3 diode in the dispersion direction (*x*-axis), which is larger than the measured offsets.

The observing plan for program 6213 was to minimize motions of the carrousel between the LSA and SSA observations. The targets were centered in the LSA and positioned into the SSA without an SSA ACQ/PEAKUP. A wavecal was obtained before each LSA observation, and the optional parameter SCISPYBAL=YES was specified for each SSA observation. A SCISPYBAL is the same as a normal SPYBAL, except it is executed at the central wavelength specified by the observer instead of the default wavelength value. There is no guarantee that the calibration lamp spectral lines will have sufficient counts for the centering program when the default central wavelengths are not used, but for program 6213, this feature is not as important as minimizing movement of the carrousel between the LSA and SSA pair of observations. Following each SSA observation and return of the target star to the LSA, an LSA ACQ/PEAKUP was specified to recenter the star in the aperture. The sequence of observations, LSA ACQ/PEAKUP, SC2 wavecal, LSA ACCUM, and SSA ACCUM, was repeated at several different central wavelengths for each grating. Even though TRANS rules (transformation of the Phase II proposal into the format used by the *HST* Planning and Scheduling software) indicate a switch from the LSA to the SSA as a new alignment, no SPYBALS were generated. The central wavelength listed in the tables is the requested central wavelength from the Phase II template.

The observations were obtained with the minimum exposures necessary to complete the respective STEP-PATT (COMB=4, FP-SPLIT=NO). Substepping using four samples per diode was performed. The diode array has five hundred 40 × 400 micron diodes on 50 micron centers. Therefore, each pixel represents a 10 micron shift.

4. Data Reduction

The SC2 wavecal was used to remove any wavelength offsets between the LSA and SSA observations due to thermal and/or geomagnetic image motion. The spectra were not smoothed or rebinned. The spectra obtained with the first order gratings G160M, G200M, and G270M were re-calibrated with the calibration switch IAC_CORR set to OMIT. The offsets were computed using cross-correlation between the LSA and SSA spectra while

keeping the SSA spectra fixed. The STSDAS tasks **taperedge, crosscor, splot,** and **gfit1d** were used to determine the relative pixel shift. The peak in the cross-correlation coefficients from the task **crosscor** was fit with a Gaussian (**splot**) and with a polynomial of order 3 (**gfit1d**). The offset was defined to be the average of these two values.

A new ccr8 table containing the average offsets was created, and as a check, the LSA observations were re-calibrated using the new table. Several absorption lines were identified in the G140M and G160M grating observations of ζ Dra (B6III). Four spectral lines were identified in both the G140M and G160M grating observations. **splot** was used to determine centroids for these spectral lines. The identified lines, vacuum wavelengths, and the measured LSA and SSA centroid wavelengths are presented in table 10. The vacuum wavelengths were obtained from Morton (1991). Although all the lines analyzed are moderately strong (except for S II 1259.519 Å), there remains small residual wavelength differences between the LSA and SSA observations. Probable sources of error for the centroids are noise in the data and systematic errors during the fitting process of each absorption line.

An interesting result which emerges from this study is a determination of the UV radial velocity of ζ Dra. The published optical radial velocity for ζ Dra from Hoffleit and Jaschek (1982) is –17V km s^{-1}, while Wilson (1963) reports a velocity of –14.1 km s^{-1} based on Lick III-prism observations. A radial velocity was calculated for each spectral line in the GHRS observations, and six of these values (excluding S II) were averaged to yield –10.9±1.4 km s^{-1}. We could not unambiguously classify the S II lines (1253.811, 1259.519 Å) as stellar features or as interstellar lines. There is a suspected feature in Al III since the 1862.7895 Å line is broadened in the blue wing. A plot of the radial velocity values versus wavelength shows a trend of decreasing radial velocity toward shorter wavelengths. This trend needs to be further investigated. An archive search for similar observations of other stars may answer this question, but unfortunately, is beyond the scope of this ISR.

A similar check was performed for the G200M and G270M grating observations. However, there were no strong absorption lines in the chosen bandpasses for comparison. Therefore, an unidentified spectral line was used for comparison between the LSA and SSA observations for each grating. For the echelle observations of χ Lupi, there were a multitude of strong absorption lines to chose from for comparison. But again, only a comparison between the LSA and SSA observations were performed. The comparisons showed similar results as for the G140M and G160M observations. These results are not presented in this ISR. We note that the radial velocity of χ Lupi could be determined once spectral lines have been identified.

5. Conclusions and Recommendations

Most exposures, except for the Ech-A observations, were very short and the SAMs (small angle maneuvers) to shift between apertures were a few seconds. The time between LSA and SSA exposures is less than ~4.5 minutes, while for Ech-A observations, the time is less than ~6.5 minutes on average. Some error may have been introduced due to the lack of SCISPYBALs and a second wavecal just before the SSA observations as well as due to the movement of the target from the LSA into the SSA, but these effects should be very small.

The results of our measurements are given in tables below for individual gratings, and summarized in Table 9 for the program as a whole. We see excellent consistency of measurement for all gratings except, perhaps, G140M, where there appears to be a trend of offset with central wavelength. The LSA ACQ and LSA ACQ/PEAKUP centering errors are ~1/3 diode in the dispersion direction (*x*-axis), which is larger than the measured offsets. The quadratic fit to the correlation values yields offsets to sub-pixel accuracy.

We determined average offsets that are different than those reported earlier by D. Lindler (GHRS-SV-108; see Table 9). We analyzed the same observations used by Lindler and got results that were very nearly the same. Thus the differences are not an artifact of analysis technique. Their origins are unclear, but in most cases the differences are not more than twice the nominal uncertainty, and so their significance is unclear. We have retained the Lindler measurements for pre-COSTAR observations, with the results of this work to be applied to post-COSTAR data.

A new ccr8 table has been created and delivered to CDBS. This table was created by coping the existing ccr8 table and editing the new table to include updated coefficients. The calibration software divides the wavelength offset coefficient *A* found in the table by the spectral order of the grating or echelle used for the observation. For the first order gratings, the wavelength offset is the incident offset coefficient *A*. But for the echelle mode, the coefficient *A* is the average offset multiplied by the respective order number (A = wavelength offset $\times m$).

6. References

Hoffleit D. and Jaschek C. 1982, The Bright Star Catalogue. Yale Univ. Observatory, Connecticut, USA.

Morton, D.C. 1991, “Atomic Data for Resonance Absorption LInes. I.Wavelengths Lanyards of the Lyman Limit”, Ap.J.Supp.Ser., 77, 119

Wilson, R.E. 1963, General Catalogue of Stellar Radial Velocities, Carnage Institution of Washington Publication 601, Washington, D.C

.

Table 3: G140M Wavelength Offsets (ζ Dra)

Observation	CARPOS	Wavelength (Å)	Aperture	SAMPLE position	Offset (pixels)	Offset (Å)
z3d50305t	17992	1250	LSA	31.20718	–0.83	–0.0116
z3d50306t			SSA	31.29281		
z3d5030bt	17648	1350	LSA	31.14412	–0.51	–0.0070
z3d5030ct			SSA	31.22975		
z3d5030ht	17336	1440	LSA	31.05666	–0.32	–0.0044
z3d5030it			SSA	31.1647		
z3d5030nt	16548	1660	LSA	30.75441	–0.22	–0.0029
z3d5030ot			SSA	30.88381		

Table 4: G160M Wavelength Offsets (ζ Dra)

Observation	CARPOS	Wavelength (Å)	Aperture	SAMPLE	Offset (pixels)	Offset (Å)
z3d50105t	51508	1250	LSA	28.68651	–2.40	–0.043
z3d50106t			SSA	28.67359		
z3d5010bt	50736	1530	LSA	28.67436	–2.31	–0.040
z3d5010ct			SSA	28.66155		
z3d5010ht	50368	1660	LSA	28.66508	–2.92	–0.051
z3d5010it			SSA	28.66128		
z3d5010nt	49820	1850	LSA	28.67915	–2.74	–0.046
z3d5010ot			SSA	28.73614		
z3d5010tt	49228	2050	LSA	28.77864	–2.68	–0.044
z3d5010ut			SSA	28.83805		

Table 5: G200M Wavelength Offsets (ζ Dra)

Observation	CARPOS	Wavelength (Å)	Aperture	SAMPLE	Offset (pixels)	Offset (Å)
z3d5010zt	25800	2050	LSA	28.65857	–2.92	–0.057
z3d50110t			SSA	28.69123		

Table 6: G270M Wavelength Offsets (ζ Dra)

Observation	CARPOS	Wavelength (Å)	Aperture	SAMPLE	Offset (pixels)	Offset (Å)
z3d50115t	10932	2050	LSA	28.69237	–2.10	–0.051
z3d50116t			SSA	28.6811		
z3d5011bt	10524	2250	LSA	28.69016	–3.14	–0.075
z3d5011ct			SSA	28.67768		
z3d5011ht	9684	2650	LSA	28.67668	–2.91	–0.067
z3d5011it			SSA	28.66343		
z3d5011nt	8916	3000	LSA	28.65597	–2.15	–0.048
z3d5011ot			SSA	28.71247		

Table 7: Echelle-A Wavelength Offsets (χ Lupi)

Observation	CARPOS	Wavelength (Å)	Aperture	SAMPLE	Order	Offset (pixels)	Offset (Å)
z3d50405t	38644	1293.0	LSA	31.99402	43	–1.77	–0.0062
z3d50406t	38644		SSA	32.1367			
z3d5040bt	38640	1635.7	LSA	30.56161	34	–2.04	–0.0090
z3d5040ct	38640		SSA	30.69018			
z3d5040ht	38644	1425.7	LSA	31.36251	39	–1.92	–0.0074
z3d5040it	38644		SSA	31.45013			
z3d5040nt	38432	1248.7	LSA	32.23469	45	–2.18	–0.0070
z3d5040ot	38432		SSA	32.36715			
z3d5040tt	38432	1440.7	LSA	31.33064	39	–1.89	–0.0071
z3d5040ut	38432		SSA	31.41561			
z3d5040zt	38200	1321.0	LSA	31.88482	43	–1.73	–0.0057
z3d50410t	38200		SSA	32.03912			
z3d50415t	38432	1652.5	LSA	30.50464	34	–2.29	–0.0098
z3d50416t	38432		SSA	30.64137			
z3d5041bt	38200	1456.3	LSA	31.29082	39	–1.93	–0.0070
z3d5041ct	38200		SSA	31.3791			
z3d5041ht	38204	1670.4	LSA	30.43213	34	–2.20	–0.0092
z3d5041it	38204		SSA	30.5699			

Table 8: Echelle-B Wavelength Offsets (χ Lupi)

Observation	CARPOS	Wavelength (Å)	Aperture	SAMPLE	Order	Offset (pixels)	Offset (Å)
z3d50205t	39356	2926.3	LSA	28.6822	19	–1.18	–0.0095
z3d50206t	39356		SSA	28.66961			
z3d5020bt	39356	2224.0	LSA	28.93883	25	–1.44	–0.0088
z3d5020ct	39356		SSA	28.92455			
z3d5020ht	39356	1793.5	LSA	28.90824	31	–1.23	–0.0060
z3d5020it	39356		SSA	28.9077			
z3d5020nt	39144	2957.9	LSA	28.67525	19	–1.63	–0.0126
z3d5020ot	39144		SSA	28.66298			
z3d5020tt	39144	2248.0	LSA	28.94242	25	–1.22	–0.0072
z3d5020ut	39144		SSA	28.91019			
z3d5020zt	39144	1812.9	LSA	28.90805	31	–1.20	–0.0057
z3d50210t	39144		SSA	28.90751			
z3d50215t	38924	2989.5	LSA	28.66807	19	–0.73	–0.0054
z3d50216t	38924		SSA	28.65569			
z3d5021bt	38924	2272.0	LSA	28.92961	25	–1.31	–0.0074
z3d5021ct	38924		SSA	28.89527			

Table 9: New LSA Incident Angle Correction for GHRS Gratings

Grating	A	B	Lindler A value
G140L	0.0	0.0	0.0
G140M	–0.0065	0.0	0.0
G160M	–0.0448	0.0	–0.022 ± 0.023
G200M	–0.057	0.0	–0.037 ± 0.012
G270M	–0.060	0.0	–0.036 ± 0.007
Ech-A	–0.0076 x *m*	0.0	0.0
Ech-B	–0.0078 x *m*	0.0	0.0

Table 10: Applying the new Offsets - Comparison of ζ Dra Spectral Lines

Spectral Lines		G140M		G160M		
Ion	**vacuum (Å)**	**LSA (Å)**	**SSA (Å)**	**LSA (Å)**	**SSA (Å)**	**velocity (km s^{-1})**
S II	1253.811	1253.753	1253.753	1253.731	1253.728	–16.63
S II	1259.519	1259.461	1259.466	1259.450	1259.445	–15.12
Si II	1526.7066	-	-	1526.647	1526.645	–11.91
Si II	1533.4312	-	-	1533.368	1533.369	–12.27
C I	1656.9283	1656.856	1656.852	1656.850	1656.888	–12.09
Al II	1670.7874	1670.722	1670.736	1670.725	1670.759	–9.32
Al III	1854.7164	-	-	1854.667	1854.658	–8.72
Al III	1862.7895	-	-	1862.725	1862.717	–11.03